Geophys. J. Int. (1994) **119,** 595–610

A continuous kinematic model of plate-tectonic motions

David Bercovici and Pål Wessel

Department of Geology and Geophysics, School of Ocean and Earth Science and Technology, University of Hawaii, Honolulu, HI 96822, *USA*

Accepted 1994 February 23. Received 1993 October 12

SUMMARY

One of the many problems in the study of plate–mantle coupling is the disparity between the theory of mantle dynamics—which involves continuum physics—and the theory of plate tectonics—which employs discontinuous plates. This discordance causes a variety of difficulties in geodynamic models, e.g. infinite tractions between the plates and mantle. As motions of the Earth's surface do not involve discontinuous plates (i.e. intraplate deformation is significant and plate margins have finite width), it is necessary to adjust the plate-tectonic model to allow for continuous surface motions. Here we present a model of plate motions on a sphere using analytically continuous (i.e. infinitely differentiable) functions to describe both plate geometry and plate margin width. We first apply this model to the idealized system of a single 'rectangular' plate to examine the influence of plate geometry and size on kinetic-energy partitioning of plate motions on a sphere. The ratio of toroidal (strike slip and spin) kinetic energy to poloidal (convergent–divergent) kinetic energy is affected not only by the relative lengths of strike-slip and convergent–divergent margins, but also on plate size, which controls the magnitude of plate spin. For large plates, spin toroidal motion contributes a major portion of the net toroidal energy. Basic concepts from this simple illustrative model are then expanded to derive an analytically continuous model of present-day plate-tectonic motions. The plate boundary for any given plate is smoothed and expressed as a single-valued differentiable function; this function is employed to generate the analytically continuous shape function of the plate. The shape function is then used to model the plate's motion about its contemporaneous Euler pole. This technique is carried out for all the plates and their motions are superposed to yield a complete yet simplified model of present-day plate motions. We use this model to examine the influence of plate margin width on energy partitioning for the Earth's plates; this approximately indicates the extent to which energy partitioning is influenced by intraplate deformation. The calculations indicate that the introduction of finite margin width allows spin vorticity to make a larger contribution to the toroidal energy. Depending on margin width, the partitioning of energy is possibly reversed, with toroidal energy assuming a larger proportion of the net kinetic energy. The model of continuous plate motions proposed here may not only ease the disparity between the theories of plate tectonics and mantle convection, but is a first simple step toward incorporating intraplate deformation into plate tectonics.

Key words: plate–mantle coupling, plate tectonics, toroidal–poloidal partitioning.

1 INTRODUCTION

The theory of plate tectonics describes motions of the Earth's lithosphere as the rotation of rigid plates on a spherical surface (Morgan 1968). While this concept has been one of the most important paradigms in the earth sciences of the century, it still presents certain intractabilities when trying to unify plate tectonics with mantle dynamics. The essence of the intractability stems from the fact that mantle dynamics is a continuum theory, whereas plate tectonics is not.

The theory of plate tectonics assumes that the boundaries between individual plates are discontinuities in the surface velocity field. While this assumption facilitates a well-determined inverse model for the determination of surface motions (e.g. Minster & Jordan 1978; DeMets *et al.* 1990), it

leads to difficulties in plate–mantle coupling models (e.g. Hager & O'Connell 1978, 1979, 1981; Olson & Corcos 1980; Ricard, Froidevaux & Fleitout 1988; Ricard & Vigny 1989; Gable, O'Connell & Travis 1991; King, Gable & Weinstein 1992) and continuum models of plate generation from mantle flow (Ribe 1992; Weinstein & Olson 1992; Bercovici 1993; see also Kaula 1980). In models of plate–mantle coupling the calculation of mantle tractions on the base of the lithosphere is essential; however, for discontinuous surface velocities, basal tractions are infinitely large, as first pointed out by Hager & O'Connell (1981). This situation can be mitigated by various *ad hoc* techniques, e.g. approximating basal tractions with ones calculated at some small depth beneath the surface (Gable *et al.* 1991). Discontinuous surface velocity fields also cause problems in combined kinematic and dynamic continuum models; in such models, lithosphere motion is driven by imposing the known divergence of plate motion as a source–sink function and determining what lithospheric rheology is necessary to yield toroidal flow most like that of the original plate (Bercovici 1993). As such models are continuous, the surface divergence must be at least second-order differentiable (and thus the velocity field must be at least third-order differentiable) to avoid singularities. However, in rigid-plate models the divergence itself is singular. Thus, differentiable or continuous plates are desirable for models of plate–mantle coupling and fluid dynamical models of plate generation. In essence, to make plate tectonics and mantle dynamics compatible, it is necessary for the tectonic model to incorporate plate continuity and therefore allow for finite plate margin width and intraplate deformation.

In this paper we present a model of plate motions that involves continuous and differentiable surface velocity fields. We use this model to examine the influence of plate shape and continuity on surface kinematics and the partitioning of kinetic energy between toroidal (strike slip and spin) and poloidal (divergent and convergent) motions. First, we give some background on kinetic-energy partitioning in surface plates. Second, we present an idealized version of the continuous-plate model to investigate some basic facets of plate kinematics and energy partitioning, such as the relative amount of toroidal energy as a function of plate geometry and size. Finally, we present a simple, continuous model of the present-day tectonic plates. The model is compared to the discontinuous plate tectonic model and is used to estimate the dependence of energy partitioning on plate continuity and plate margin width.

2 TOROIDAL AND POLOIDAL MOTIONS AND KINETIC-ENERGY PARTITIONING ON A SPHERE

The motion of the Earth's tectonic plates can be divided into two components: toroidal motion, involving vertical vorticity in the forms of spin and strike-slip shear, and poloidal motion, involving convergence and divergence. The kinetic energy of plate motions was first noted by Hager & O'Connell (1978) to be nearly equipartitioned between toroidal and poloidal parts. This partitioning is one of the primary issues in the effort to link plate tectonics and mantle convection (e.g. see Hager & O'Connell 1978, 1979; Kaula 1980; Forte & Peltier 1987; Gable *et al.* 1991; O'Connell, Gable & Hager 1991; Olson & Bercovici 1991; Christensen & Harder 1991; Ribe 1992; Bercovici 1993).

It is necessary to understand the manner in which the size, geometry and strength distribution of the plates are related to their kinetic-energy partitioning. Kaula & Williams (1983) and Forte & Peltier (1987) interpreted the poloidal energy as associated with convergent–divergent margins, while toroidal energy is associated with transform faults. It is in fact more general to associate toroidal motion with strike-slip margins that also include oblique subduction zones; one of the largest highs in vertical vorticity occurs over the Java trench. In Cartesian geometry, kinetic-energy partitioning is fairly predictable. For plates undergoing simple drift (i.e. all translation and no spin) the amount of toroidal energy is independent of plate size and entirely dependent on plate geometry; i.e. the longer the strike-slip margins are relative to the convegent–divergent margins, the greater the proportion of toroidal energy (Olson & Bercovici 1991; O'Connell *et al.* 1991). The near equipartitioning of the Earth's kinetic energy has thus been interpreted as characteristic of a system of many small plates with a random distribution of geometries or a few plates that are primarily equidimensioned (i.e. square) (Olson & Bercovici 1991; Ribe 1992). However, the Earth's kinetic energy is strongly dominated by the Pacific plate which is neither small nor square. The geometrical interpretation of the Earth's kinetic-energy partitioning is somewhat flawed because of the assumption of pure drifting motion and its basis in Cartesian geometry. For motion on a sphere, it is not possible to separate plate drift and spin since the only part of a plate that does not spin is the line of points 90° from the Euler pole. Plate spin is manifest as toroidal motion, and the larger a plate the greater the contribution of spin to toroidal energy. The dependence of kinetic-energy partitioning on plate geometry is therefore not as simple as Cartesian models imply and plate size plays a distinct role. In order to understand the effects of plate continuity in this paper, we first systematically categorize the influence of plate shape and size on kinetic-energy partitioning for spherical geometry (Section 4).

Related to the presence of spin is the net rotation of the lithosphere. Net lithosphere rotation is manifest as toroidal motion with spherical-harmonic degree $\ell = 1$. However, the amount of lithospheric rotation is also reference-frame dependent. In models of plate motions (Minster *et al.* 1974; Minster & Jordan, 1978; DeMets *et al.* 1990) the Euler poles can only be calculated relatively. Absolute plate motions require a choice of reference frame which is somewhat subjective. The classical and perhaps best reasoned choice is that of the hotspot reference frame. The $\ell = 1$ toroidal power in the hotspot reference frame is continuous with the rest of the spherical-harmonic spectrum, providing relatively empirical support for this choice of frame (since a different choice would cause the $\ell = 1$ power to be anomalously out of line with the rest of the spectrum) (O'Connell *et al.* 1991). Even so, the observation that net lithospheric rotation in the hotspot frame is extremely slow has lead to the suggestion that an equally viable reference frame is one that has zero net rotation (Minster *et al.* 1974). Some investigators have argued that since net rotation is frame dependent it is physically meaningless and thus should be removed from interpretations of kinetic-energy partitioning (Lithgow-

Bertelloni *et al.* 1993). This argument has lead to the conclusion that the present-day plate kinetic energies are far from equipartitioned, i.e. the toroidal component of kinetic energy is perhaps only 30 per cent of the poloidal component. However, a rotating frame does not obey Galilean invariance, thus neglect of net rotation by appealing to frame independence is specious. Moreover, there is no reason that mantle convective stresses cannot induce net rotation of the lithosphere (O'Connell *et al.* 1991). Therefore, given the ambiguity over the treatment of net rotation, we consider frames of reference with and without net rotation while examining the relation between kinetic-energy partitioning and plate geometry.

3 THEORY

3.1 Kinematics of a continuous plate on a sphere

The surface velocity field associated with the motion of a single plate on the surface of a sphere is

$$\mathbf{v} = \boldsymbol{\Omega} \times \mathbf{R}S(\theta, \phi) \tag{1}$$

where $\boldsymbol{\Omega}$ is the constant angular velocity vector that intersects the surface of the sphere at the Euler pole; $\mathbf{R} = R\hat{r}$ is the position vector of an arbitrary point on the sphere of radius R; θ and ϕ are colatitude and longitude, respectively, and $\hat{r}$ is the unit radial vector at θ and ϕ. S is the shape function of the plate that prescribes both the figure of the plate and the sharpness of its boundaries; S is unity at the centre of the plate and goes to zero outside the plate boundary (see Section 3.2).

It is most convenient to express $\boldsymbol{\Omega}$ in Cartesian components, i.e. $\boldsymbol{\Omega} = (\Omega_x, \Omega_y, \Omega_z)$ where the z axis points through the geographic north pole and the x axis points through the intercept of the zero meridian and the equator. The horizontal divergence and radial vorticity at the surface are, respectively,

$$D = \nabla_h \cdot \mathbf{v} = \Omega_\phi \frac{\partial S}{\partial \theta} - \Omega_\theta \frac{1}{\sin\theta} \frac{\partial S}{\partial \phi} \tag{2}$$

$$\omega_r = \hat{r} \cdot \nabla \times \mathbf{v} = 2S\Omega_r - \Omega_\theta \frac{\partial S}{\partial \theta} - \Omega_\phi \frac{1}{\sin\theta} \frac{\partial S}{\partial \phi} \tag{3}$$

where

$$\Omega_r = (\Omega_x \cos\phi + \Omega_y \sin\phi)\sin\theta + \Omega_z \cos\theta \tag{4}$$

$$\Omega_\theta = (\Omega_x \cos\phi + \Omega_y \sin\phi)\cos\theta - \Omega_z \sin\theta \tag{5}$$

$$\Omega_\phi = \Omega_y \cos\phi - \Omega_x \sin\phi \tag{6}$$

are the angular velocity components in spherical coordinates. For plates undergoing pure drift in a Cartesian geometry, the expressions for divergence and vorticity have an antisymmetrical appearance (Olson & Bercovici 1991); in spherical geometry this symmetry is broken by the first term on the right side of eq. (3), (i.e. the term proportional to S). This term represents the spin vorticity of a point on the surface at position (θ, ϕ); thus the contribution of spin cannot be eliminated from plate motion on a sphere. All other terms in the expressions for divergence and vorticity involve transitions in velocity at the plate boundaries (i.e., where S changes from unity to zero).

To determine kinetic-energy partitioning, we separate the surface velocity field into poloidal and toroidal parts by a Helmholtz representation:

$$\mathbf{v} = \nabla_h \Phi + \nabla \times (\Psi \hat{r}) \tag{7}$$

where Φ is the poloidal scalar potential and $\Psi\hat{r}$ is the toroidal vector potential. The poloidal velocity $\nabla_h\Phi$ is irrotational on the surface of the sphere while the toroidal velocity $\nabla \times (\Psi\hat{r})$ is solenoidal both on the surface of the sphere and throughout the volume of the sphere. Using this relation, the horizontal divergence and radial vorticity of the velocity field are

$$\nabla_h^2 \Phi = D, \qquad \nabla_h^2 \Psi = -\omega_r \tag{8}$$

respectively, thus yielding two Poisson's equations for the poloidal and toroidal potentials. To find Φ and Ψ given D and ω_r from eqs (2) and (3) we represent all variables with spherical-harmonic expansions, e.g.

$$D = \sum_{\ell=0}^{\infty} \sum_{m=-\ell}^{+\ell} D_{\ell m} Y_{\ell m} \tag{9}$$

where

$$D_{\ell m} = \int_0^{2\pi} \int_{-1}^{+1} D(\theta, \phi) Y_{\ell m}^* \, d(\cos\theta)\, d\phi \tag{10}$$

is a complex coefficient and $Y_{\ell m}$ is a normalized complex spherical harmonic of degree ℓ and order m. By definition of a spherical harmonic, $R^2\nabla_h^2 Y_{\ell m} = -\ell(\ell+1)Y_{\ell m}$, thus eq. (8) leads to

$$(\Phi_{\ell m}, \Psi_{\ell m}) = \frac{R^2}{\ell(\ell+1)}(-D_{\ell m}, \omega_{\ell m}). \tag{11}$$

The kinetic energy per unit mass integrated over the surface of the sphere is

$$KE = \frac{R^4}{2} \sum_{\ell m} \frac{1}{\ell(\ell+1)} (|D_{\ell m}|^2 + |\omega_{\ell m}|^2) \tag{12}$$

where the first and second terms on the right of eq. (12) are the poloidal and toroidal kinetic energies, KE_P and KE_T, respectively. Thus, the toroidal–poloidal kinetic-energy ratio is

$$KE_T/KE_P = \frac{\sum_{\ell m} \frac{1}{\ell(\ell+1)} |\omega_{\ell m}|^2}{\sum_{\ell m} \frac{1}{\ell(\ell+1)} |D_{\ell m}|^2}. \tag{13}$$

This ratio is the primary measure of kinetic-energy partitioning for plate motions.

3.2 The plate-shape function

In the theory of plate tectonics, the shape function S for each plate is a discontinuous step function; the divergence and vorticity at plate margins are thus singularities. A

discontinuous plate shape function is essentially composed of linear step-functions

$$s(x, x_0, b) = \begin{cases} 0 & \dfrac{x - x_0}{b} < -1 \\ 1 & -1 \le \dfrac{x - x_0}{b} \le 1 \\ 0 & \dfrac{x - x_0}{b} > 1 \end{cases} \tag{14}$$

(where the step function is centred on x_0 and has half-width b). For a continuous plate, s is replaced with an analytic, infinitely differentiable function. For versatility, we employ a shape function in which plate size and margin width can be independently prescribed; e.g.

$$s(x, x_0, b) = \frac{\tanh\left(\dfrac{x - x_0 + b}{\delta}\right) - \tanh\left(\dfrac{x - x_0 - b}{\delta}\right)}{2\tanh(b/\delta)} \tag{15}$$

where x_0 and b have their previous definitions and δ is the margin half-width. Divergence and vorticity depend on the derivative of this function, e.g.

$$\frac{ds}{dx} = \frac{\operatorname{sech}^2\left(\dfrac{x - x_0 + b}{\delta}\right) - \operatorname{sech}^2\left(\dfrac{x - x_0 - b}{\delta}\right)}{2\delta \tanh(b/\delta)} \tag{16}$$

with extrema at $x = x_0 \pm b$. Functions other than hyperbolic tangents could be used for s, e.g. error functions for which the squared hyperbolic secants of eq. (16) would be replaced by Gaussians.

It should be emphasized that the plate-shape function is not based on any physical model for intraplate deformation. These plate models are intended to be a simple parametrization of plate continuity, which is in itself only a crude approximation of intraplate deformation. Rigorous incorporation of intraplate deformation is beyond the scope of this paper, but is conceivable within the framework presented here (see Section 6).

4 ENERGY PARTITIONING FOR IDEALIZED PLATES

The simplest idealization of a tectonic plate is a single, four-sided plate translating across the surface of a sphere in a direction perpendicular to two of its boundaries and parallel to the other two. Convergence and divergence (i.e. poloidal motion) are confined to the leading and trailing boundaries, respectively, and strike-slip vorticity is confined to the other two boundaries. We can therefore identify specific boundaries as either convergent–divergent or strike slip, and thus systematically discern the dependence of kinetic-energy partitioning on plate geometry.

We accomplish this idealization by specifying the plate's Euler pole to be 90° from its centre of figure. (The Earth's major energy carrying plates in fact have similarly large angles between their Euler poles and centres of figure; see Olson & Bercovici 1991.) Furthermore, the geographic north pole is chosen to coincide with the Euler pole; thus, for motion to be entirely perpendicular or parallel to the boundaries, the boundaries must lie on lines of constant latitude or longitude. The strike-slip boundaries therefore lie on small circles of constant latitude and the convergent–divergent boundaries lie on meridians. We call such a plate 'rectangular' or 'square', where the quotation marks indicate that these geometries are in the spherical sense.

The angular velocity vector has only one component, i.e., $\boldsymbol{\Omega} = \Omega_z \hat{z}$ such that motion is only in the $\hat{\phi}$ direction. The centre of figure of the plate lies on the equator and at $\phi = \pi$. For the shape of this plate we use the product of two linear shape functions from eq. (15) such that

$$v_\phi = \Omega_z R \sin\theta s(\phi, \pi, \alpha) s\left(\theta, \frac{\pi}{2}, \beta\right) \tag{17}$$

$$D = \Omega_z s\left(\theta, \frac{\pi}{2}, \beta\right) \frac{ds(\phi, \pi, \alpha)}{d\phi} \tag{18}$$

$$\omega_r = \Omega_z s(\phi, \pi, \alpha) \frac{1}{\sin\theta} \frac{d}{d\theta}\left[\sin^2\theta s\left(\theta, \frac{\pi}{2}, \beta\right)\right] \tag{19}$$

where α and β are the angular half-widths of the plates in the longitudinal and latitudinal directions, respectively. The same margin half-width δ is used in both directions. Fig. 1 shows an example of the plate velocity, divergence and vorticity fields. To investigate kinetic-energy partitioning, we determine coefficients $D_{\ell m}$ and $\omega_{\ell m}$ numerically by Gaussian quadrature in latitude and fast Fourier transforms in longitude. In the following subsection we will examine the basic relationships between kinetic-energy partitioning and simple plate geometry.

4.1 Energy partitioning for a 'rectangular' plate

We first consider the kinetic-energy partitioning of a general 'rectangular' plate for a full range of plate half-widths α and β. In all cases we take R and Ω_z to be unity, and $\delta = \pi/90$. Fig. 2 shows KE_P, KE_T and KE_T/KE_P versus α and β. As expected, poloidal kinetic energy KE_P increases with β for a given α as the convergent–divergent margins increase in size (Fig. 2a). However, for a fixed β, KE_P changes non-monotonically with strike-slip margin size α, especially for the larger β. This trend is distinctly different from Cartesian cases (Olson & Bercovici 1991) for which KE_P is independent of strike-slip margin length. This relation occurs because as α approaches either 0 or π, the regions of divergence and convergence begin to cancel each other (i.e. the plate either becomes vanishingly narrow or closes on itself), thus reducing the amount of poloidal flow.

In the frame of reference with solid-body or net rotation, the toroidal kinetic energy KE_T increases monotonically with α, or strike-slip margin length, as expected (Fig. 2b). For fixed α and increasing β, strike-slip shear decreases since, as the strike-slip margins approach the Euler pole, the velocity at these margins vanishes. Even so, KE_T increases with β (and α fixed) because the contribution of spin to the toroidal motion increases as the plate becomes larger. Again this differs from Cartesian models wherein KE_T is independent of convergent–divergent margin size.

In the frame of reference without solid-body or net rotation (Fig. 2b), KE_T increases monotonically with strike-slip margin length (α) only for small values of β. For values of $\beta > 0.222\pi$ (i.e. 40°), KE_T reaches a maximum value with increasing strike-slip margin length α, and then decreases for $\alpha > 0.556\pi$ (i.e. 100°). This maximum occurs because the spin vorticity, which makes the primary contribution to toroidal energy for large plates, is largely removed in the no-net-rotation frame; thus as the plate size approaches that of the entire lithosphere the toroidal energy

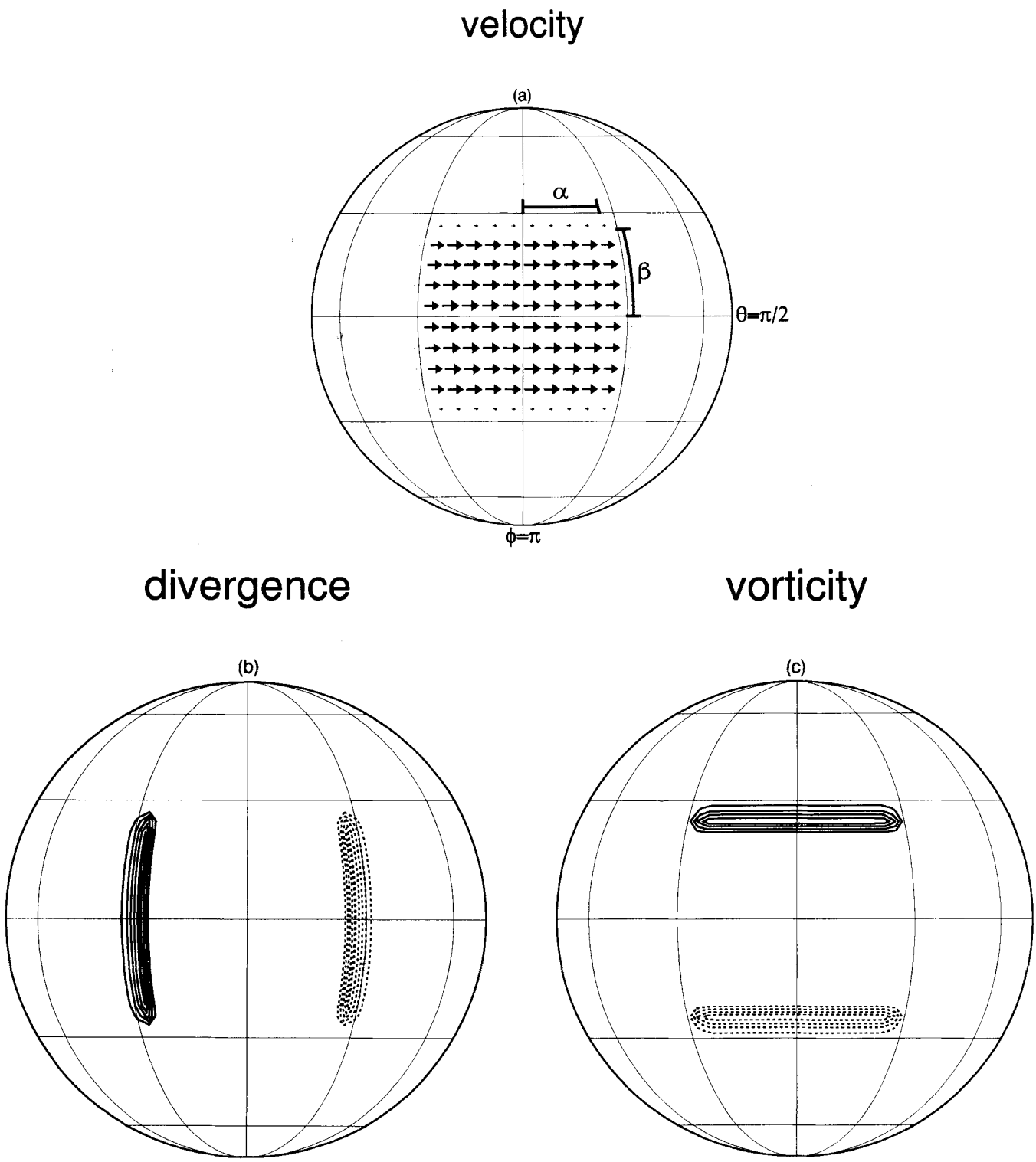

Figure 1. Velocity field (a), horizontal divergence (b) and radial vorticity (c) of an idealized 'rectangular' plate on a sphere for $\alpha = \beta = 5\pi/36$ (i.e. 25°) and $\delta = \pi/90$ (i.e., 2°). Solid (dashed) contours indicate positive (negative) values. Angular velocity Ω_z and sphere radius R are set equal to 1, thus the maximum velocity vector is 1. The minimum and maximum contours for the divergence and vorticity fields are ±12.89 and 12.08, respectively; the contour interval is 2.5 for both fields.

vanishes. The influence of spin kinetic energy is also obvious in Fig. 2(b) from the fact that the maximum KE_T with net rotation is approximately five times larger than the maximum KE_T without net rotation. Although the no-net-rotation frame has no clear physical justification, this exercise serves to illustrate that spin vorticity makes the primary contribution to toroidal energy for large plates.

The ratio between the toroidal and poloidal kinetic energies KE_T/KE_P is shown in Fig. 2(c). In the reference frame with net rotation, KE_T/KE_P increases as strike-slip

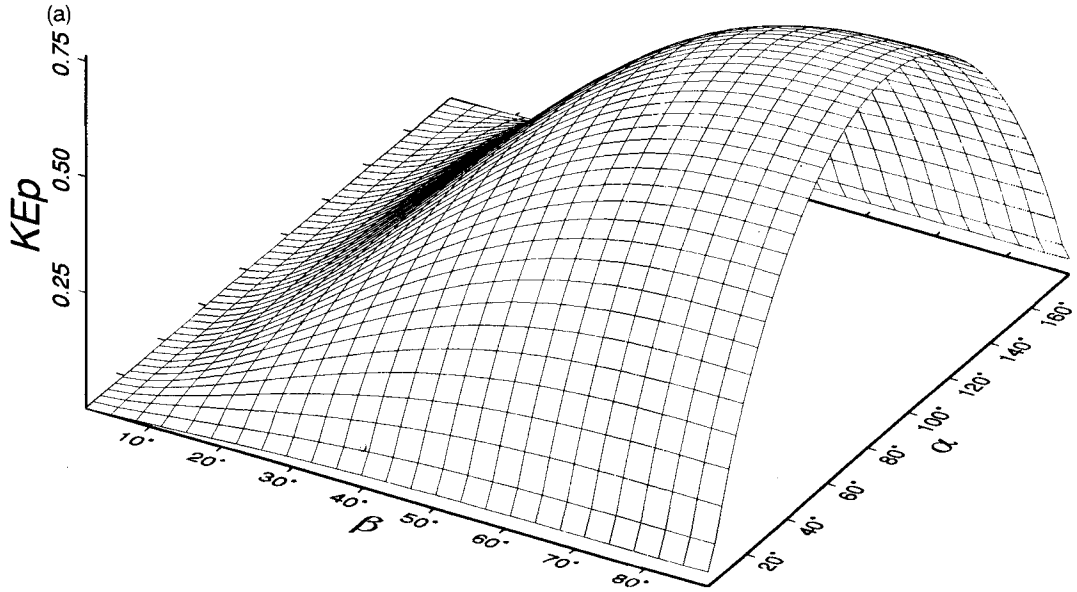

Figure 2. Poloidal kinetic energy KE_P (a), toroidal kinetic energy KE_T with and without solid-body (or net) rotation (SBR) (b), and the energy partitioning ratio KE_T/KE_P with and without SBR (c) versus margin half-widths α and β (shown in degrees) for the idealized 'rectangular' plate translating eastward as in Fig. 1. In all cases $\delta = \pi/90$ (i.e. 2°). The thick black curve on (c) indicates values for the 'square' plate, wherein all margins have the same arc-length; shading indicates the level of equipartitioning, where the contour line separating gray and white indicates $KE_T/KE_P = 1$. Kinetic energy is dimensionless in that the angular velocity Ω_z and the sphere radius R are unity.

margin length (α) and plate size increase for all fixed β. The ratio approaches a singularity as $\alpha \to \pi$ (this is not obvious from the figure which employs a $\log_{10}$ scale) since the poloidal energy vanishes as the leading and trailing edges of the plate connect while the toroidal energy remains finite. For fixed strike-slip margin length (α), the ratio decreases as the convergent–divergent margin length β increases. This trend actually displays three combined effects: as β increases, poloidal and spin toroidal energies increase while strike-slip toroidal energy decreases. In the Cartesian model of Olson & Bercovici (1991), KE_T/KE_P is only a function of the ratio of strike-slip margin length to convergent–divergent margin length; i.e. the ratio is only dependent on the aspect ratio of the plate. As shown by Fig. 2(c), this simple relation does not hold in a spherical geometry; for plate motion on a sphere, the kinetic-energy partitioning depends on plate size as well as geometry.

In the no-net-rotation frame, the kinetic-energy ratio essentially reflects the toroidal energy (Fig. 2c). For small α and β the ratio KE_T/KE_P behaves as in the reference frame with net rotation. For large values of α and β, however, KE_T/KE_P approaches zero as plate size increases, even though both KE_T and KE_P in this frame go to zero in the limit of a global plate ($\alpha = \pi$, $\beta = \pi/2$). (This trend occurs because as the global-plate limit is approached, the strike-slip margins vanish by dual effects, i.e. they shorten and close up at the poles; in contrast, the convergent–divergent margins become very long and only vanish as the leading and trailing plate edges connect.) These results suggest that the low value of KE_T/KE_P obtained for the Earth's plates in the no-net-rotation frame (Lithgow-Bertelloni *et al.* 1993) simply occurs because the spin energy of the large fast plates (in particular, the Pacific plate) is essentially removed in this frame.

The influence of spherical geometry on kinetic-energy partitioning is well illustrated by examining the kinetic energies for a 'square' plate in which all four boundaries have equal arc-length. As mentioned above, the kinetic energy for a square plate in a Cartesian geometry is equipartioned between toroidal and poloidal parts (i.e. $KE_T/KE_P = 1$) regardless of plate size and velocity (Olson & Bercovici 1991) because the strike-slip and convergent–divergent margins have all the same lengths. However, while a 'square' plate on a sphere may maintain similar unity aspect ratio, the kinetic-energy partitioning will change as its size varies. For a 'square' plate, α is a function of β:

$$\alpha = \beta/\cos\beta. \tag{20}$$

Since $\alpha \leq \pi$, the constraint that $\beta/\cos\beta \leq \pi$ is more restrictive than $\beta \leq \pi/2$. This constraint leads to $\beta \leq 0.377\pi$ (or $\beta \leq 67.85°$); at $\beta = 0.377\pi$ the trailing and leading edges of the 'square' plate connect. The curve defined by eq. (20) is projected onto the surfaces of KE_T/KE_P versus α and β (Fig. 2c). Shading on these surfaces indicate the level of equipartitioning (gray indicates where $KE_T/KE_P < 1$, white where $KE_T/KE_P > 1$). This exercise demonstrates that, in contrast to the Cartesian case, KE_T/KE_P for 'square' plates is not constant at unity except for very small plates. For cases with net rotation, the ratio exceeds unity as plate size increases. For cases in the no-net-rotation frame, the ratio is less than unity as plate size increases, except near the singularity at $\beta = 0.377\pi$ where $KE_P \to 0$.

5 A CONTINUOUS MODEL OF THE TECTONIC PLATES

In this section we introduce a model of the present-day tectonic plates that involves analytically continuous, infinitely differentiable plate-shape functions. This model is

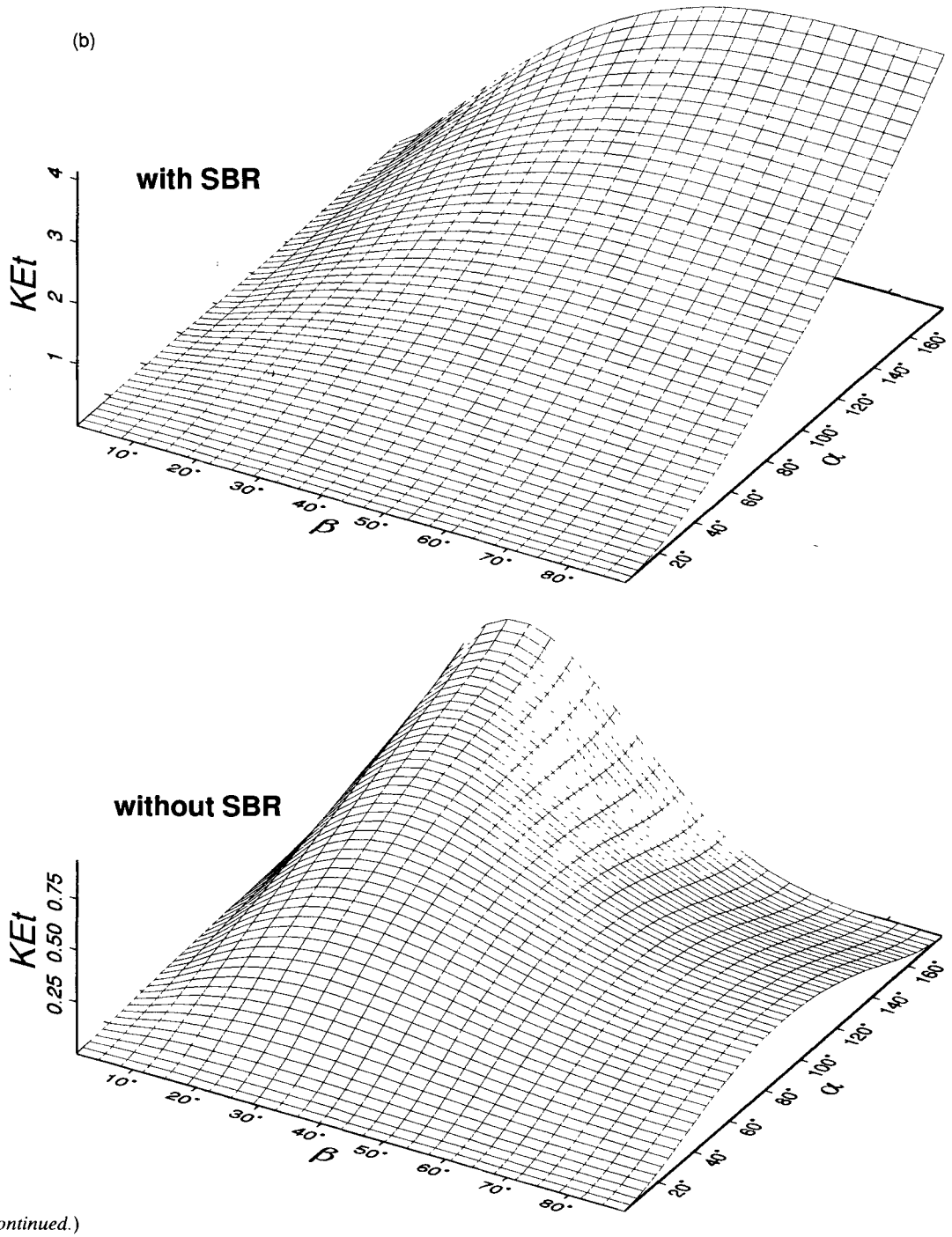

Figure 2. (*Continued.*)

desirable in many aspects over a spherical-harmonic representation of discontinuous plates (Hager & O'Connell 1978, 1979, 1981; O'Connell *et al.* 1991). Spherical-harmonic analyses are well behaved in representing the toroidal and poloidal functions Ψ and Φ. However, divergence and vorticity for the discontinuous-plate model are singularities and their spherical-harmonic representations are non-convergent series; their amplitudes are thus dependent on series truncation and they exhibit considerable Gibbs effects, i.e. ringing. Fig. 3 shows a spherical-harmonic model of divergence and vorticity derived from the NUVEL-1 discontinuous plate model (DeMets *et al.* 1990; O'Connell, personal communication, 1992). Ringing is particularly noticeable in the divergence field around the East Pacific Rise, and in the vorticity field on the Phillipine plate. Numerical convergence and Gibbs phenomena are greatly reduced or eliminated altogether in the model presented here since divergence and vorticity are not singularities. More importantly, actual data on intraplate deformation and margin width could be incorporated into this model.

We first present the mathematical model of continuous tectonic plates and then use it to examine the influence of plate margin width on kinetic-energy partitioning of the Earth's surface motions.

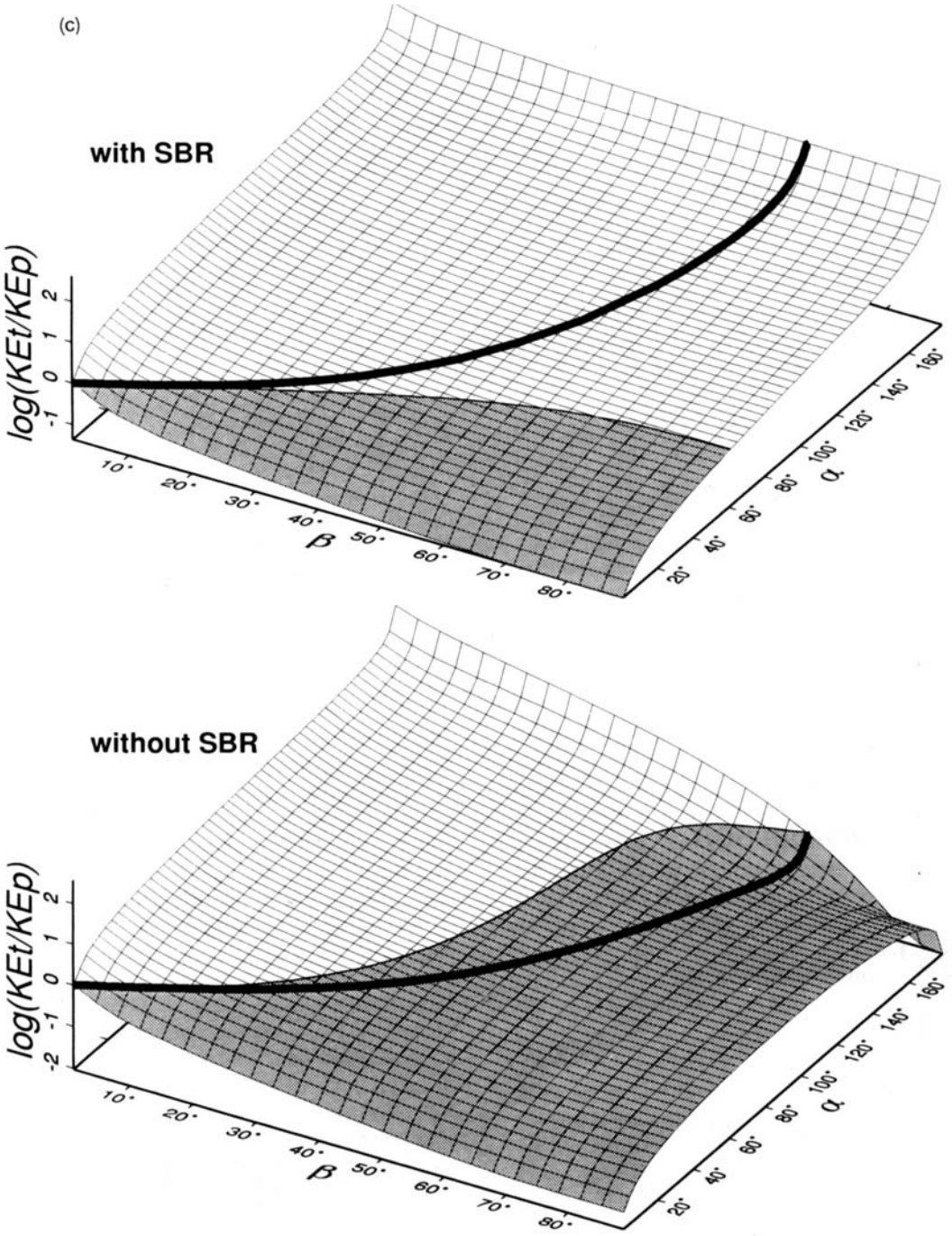

Figure 2. (*Continued.*)

5.1 Mathematical model

The angular velocities of the present-day plates is determined from the NUVEL-1 Pacific-plate-fixed Euler poles (DeMets *et al.* 1990; see also DeMets 1993) added to estimates of the instantaneous Pacific-hotspot pole from Pollitz's (1988) joint inversion of North American and Pacific plate motions. The surface velocity field of the 12 primary plates is expressed with a single equation:

$$\mathbf{v} = -\mathbf{R} \times \sum_{i=1}^{12} \mathbf{\Omega}_i S_i(\theta, \phi) \tag{21}$$

where $\mathbf{\Omega}_i$ and S_i are the angular velocity vector and shape function of the ith plate, respectively. The procedure for determining S_i is the most crucial aspect of the model; we thus discuss it as a sequence of steps.

Step 1: plate-boundary filtering

To make the model of the tectonic plates analytically continuous, the plate boundaries must be smoothed. This is necessary for two reasons. First, boundary offsets (e.g. transform faults) are analytically intractable. Second, large

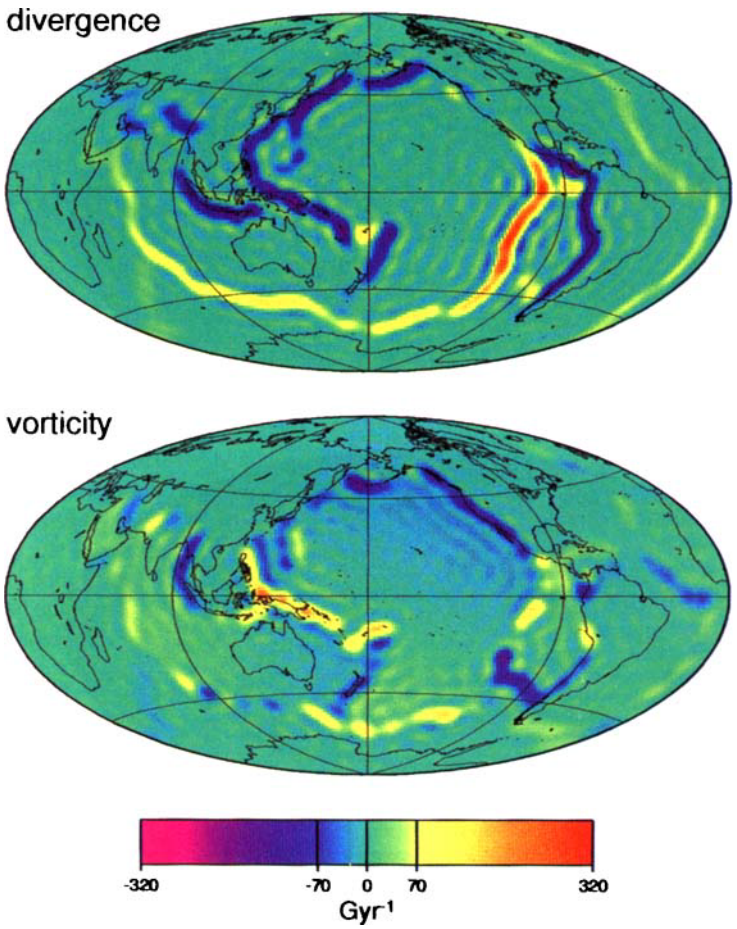

Figure 3. Horizontal divergence and radial vorticity for the discontinuous plate-tectonic model (derived from a spherical-harmonic analysis of the NUVEL-1 model; O'Connell, personal communication, 1992).

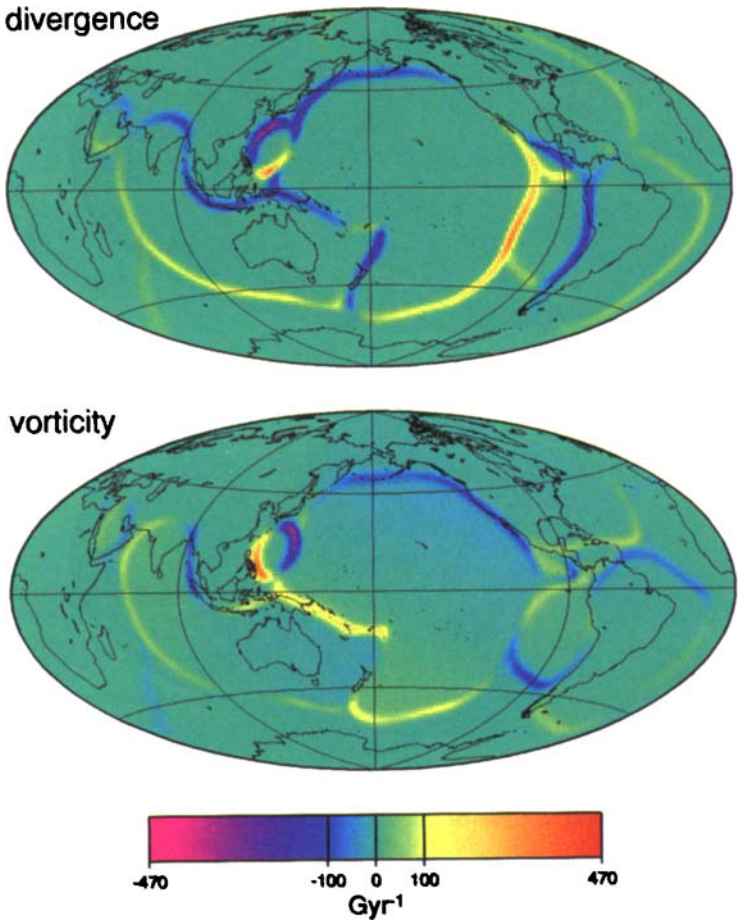

Figure 5. Horizontal divergence and radial vorticity for the continuous plate model with margin width $R\delta = 200$ km.

changes in boundary curvature (e.g. the Indo–Australian and North American plates) cause a non-analytic plate shape function; this point is more fully explained in Step 3 below. Thus, both discontinuities and large changes in curvature are smoothed out. Filtering is accomplished by representing the latitude and longitude of boundary points as two separate, discrete, single-valued functions of distance along the boundary. These two series are then smoothed by spatially convolving them with a Gaussian filter of a particular half-width. After the filtering, the latitude and longitude data are recombined to yield smoothed plate boundaries (Fig. 4a). The choice of Gaussian-filter half-width depends on being able to analytically describe the plate boundary (again, see Step 3 below). The plate boundaries do not overlap so long as the same Gaussian-filter half-width is used for all the plates. However, because plate boundaries are rounded, gaps between plates unavoidably occur. This effect is particularly noticeable for small plates which are significantly reduced in size by the boundary filtering (Fig. 4a).

Step 2: plate-boundary rotation

The filtered plate-boundary data are then rotated into a frame of reference where the plate centre of figure is at longitude π and colatitude $\pi/2$ (Fig. 4b). (The plate centre of figure is defined as the centre of 'mass' of evenly spaced boundary points; it is thus prudent to resample the boundary data to be evenly spaced in distance.) This rotation assures that the plate-shape function is defined in a coordinate system where the plate does not contain a geographic pole and where the plate boundary does not cross the zero meridian. The new coordinate system is denoted by (θ', ϕ') and is unique to each plate.

Step 3: the plate-boundary function

For a given plate (see Fig. 4c), the pseudo-distance from an arbitrary point within the plate (θ_0', ϕ_0') to any other point on the globe (θ', ϕ') is

$$\Delta(\theta', \phi') = \sqrt{(\phi' - \phi_0')^2 + (\theta' - \theta_0')^2}. \tag{22}$$

The pseudo-angle between the line connecting these two points and the line connecting (θ_0', ϕ_0') and the first plate-boundary data point $(\theta_{b_1}', \phi_{b_1}')$ is

$$\lambda = \tan^{-1}\left(\frac{\theta' - \theta_0'}{\phi' - \phi_0'}\right) - \tan^{-1}\left(\frac{\theta_{b_1}' - \theta_0'}{\phi_{b_1}' - \phi_0'}\right). \tag{23}$$

(The terms 'pseudo-distance' and 'pseudo-angle' are used because these quantities treat θ' and ϕ' as if they were Cartesian coordinates; since this model is a purely mathematical description of an arbitrary shape, accounting for spherical curvature at this level of the model is an unnecessary complication.) An arbitrary boundary point (θ_b', ϕ_b') has pseudo-distance $\Delta_b = \Delta(\theta_b', \phi_b')$. In order to make the plate shape analytically continuous, Δ_b must be expressed as a single-valued function in λ; this function $\Delta_b(\lambda)$ is called the *plate-boundary function*. Achieving a single-valued $\Delta_b(\lambda)$ requires a prudent choice of (θ_0', ϕ_0') in conjunction with sufficient smoothing of the boundary. For a given plate, we search for the optimum (θ_0', ϕ_0'); since multivalued functions have singularities in their slope, the optimum (θ_0', ϕ_0') is defined as one that yields the smallest maximum in $|d\Delta_b/d\lambda|$. However, unless the boundary is adequately smoothed, even this $|d\Delta_b/d\lambda|$ is infinite, or very nearly so. Thus, we also find the minimum Gaussian-filter width which yields a finite value for the smallest maximum in $|d\Delta_b/d\lambda|$. Since the same filter width should be used for every plate (to preclude overlap), the largest filter width amongst all plates is used. In this sense, the Indo–Australian plate is the most restrictive given its elongated shape and change in boundary curvature from convex within the Himalayan Plateau to concave at the Java trench. The Gaussian-filter half-width, therefore, must be at least 7000 km for the $\Delta_b(\lambda)$ of each plate to be single-valued. The plate-boundary function $\Delta_b(\lambda)$ is then evenly resampled in λ with radix-2 number of points and discrete Fourier transformed to obtain $\tilde{\Delta}_n$ such that

$$\Delta_b(\lambda) = \frac{1}{N}\sum_{n=-N/2}^{N/2} \tilde{\Delta}_n e^{in\lambda} \tag{24}$$

and N is the number of resampled points. In this way, $\Delta_b(\lambda)$ is expressed as an analytic function. Therefore, for any given point on the surface of the sphere with coordinates (θ', ϕ'), the function $\Delta_b[\lambda(\phi', \theta')] - \Delta(\phi', \theta')$ is greater than, equal to, or less than zero depending on whether the point is inside, on, or outside the boundary, respectively.

Step 4: the plate-margin function

The shape function S of any plate is given by

$$S(\theta', \phi') = \frac{1}{2}\left[1 + \tanh\left(\frac{\Delta_b(\lambda) - \Delta}{\delta^*(\lambda)}\right)\right] \tag{25}$$

where $\delta^* < \bar{\Delta}_b = \tilde{\Delta}_0/N$. (The quantity $\bar{\Delta}_b$ represents the characteristic mean pseudo-radius of the given plate). The function $\delta^*(\lambda)$ is the plate margin half-width (in the pseudo-coordinates employed here, with units of radians) along the line connecting the points (θ_0', ϕ_0') and (θ', ϕ'); δ^* *is not the margin width normal to the boundary.* As this model attempts to include information about plate continuity and margin width, δ^* represents the significant new parameter added to the plate-tectonic model. It is through δ^* that data on intraplate deformation could be conceivably incorporated. Presently δ^* is unconstrained. For consistency with the plate-tectonic model, we would ideally have the margin width be constant normal to the boundary. However, for simplicity we approximate this condition by prescribing the margin in $\Delta - \lambda$ space (i.e. treating Δ and λ as Cartesian coordinates) to be uniformly thick (Fig. 4d). With the plate boundary described in this space by the curve $\Delta_b(\lambda)$, the normal to the boundary has angle

$$\nu = \tan^{-1}\left[-\left(\frac{d\Delta_b}{d\lambda}\right)^{-1}\right] \tag{26}$$

relative to the λ-axis. The line drawn from (θ_0', ϕ_0') to the boundary is a line of constant λ and thus a vertical line in Δ–λ space; this line intersects the boundary at an angle to the boundary normal of $(\pi/2) - \nu$. If the margin has a

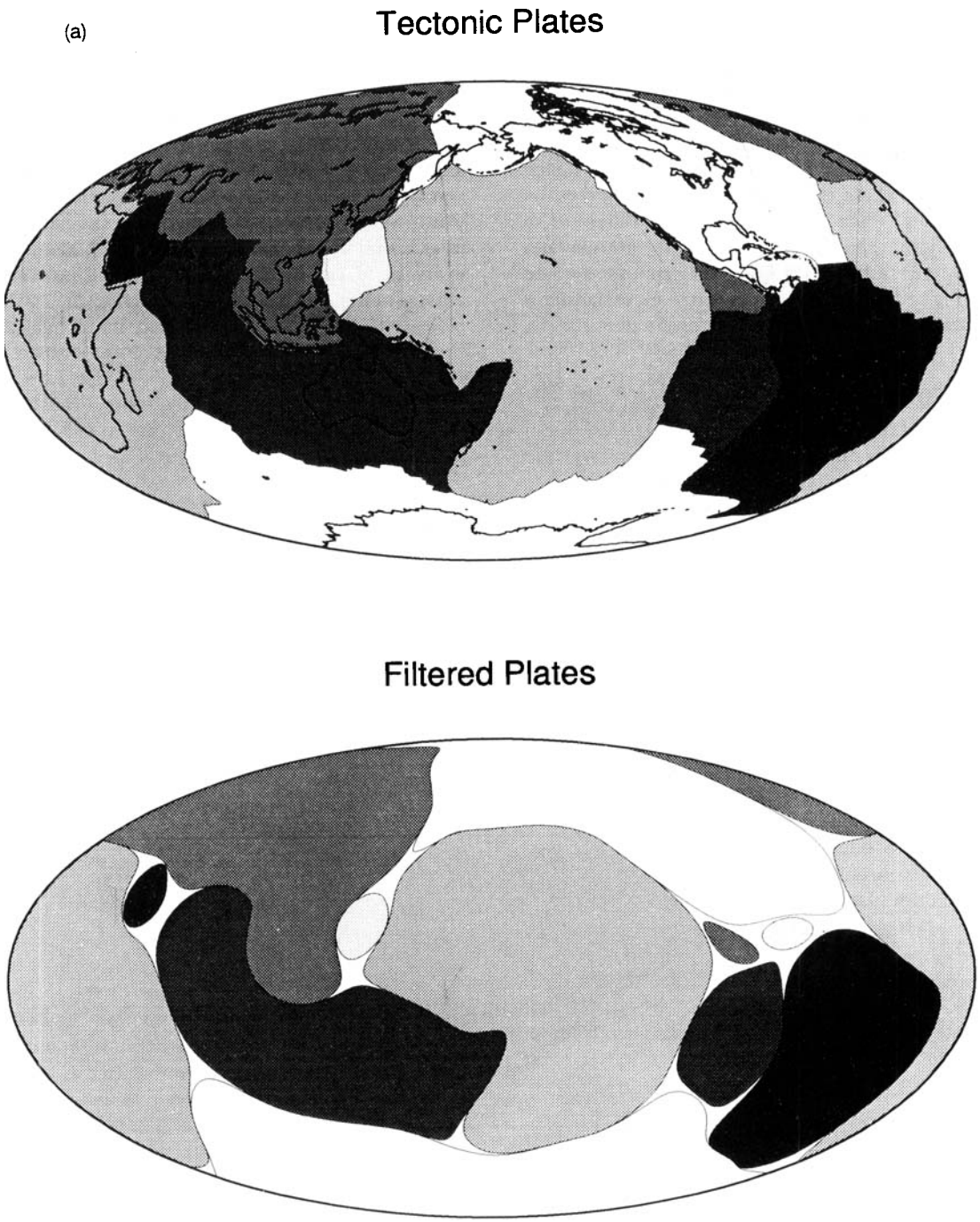

Figure 4. Illustration of the procedure for constructing the analytically continuous model of present-day plate motions.

(a) Outline of present-day plate geometries before (top frame) and after (bottom frame) smoothing of the boundaries.

(b) Illustration of rotation of a plate into a reference frame where the centre of figure of the plate lies at the equator and the 180° meridian. The plate shown here and subsequently is the North American plate. The white and gray plates are its original (geographic) and rotated positions, respectively.

(c) Illustration of the coordinates describing the plate-boundary function; see text for discussion.

(d) Illustration for the simplified definition of the plate-margin function; see text for discussion.

constant width δ normal to the boundary (in Δ–λ space), then the margin width along the constant-λ line is

$$\delta^* = \frac{\delta}{|\sin \nu|} = \delta \sqrt{1 + \left(\frac{d\Delta_b}{d\lambda}\right)^2}. \tag{27}$$

Allowing for the margin width to be constant normal to the boundary in more realistic coordinates, e.g. accounting for spherical curvature, is possible through a similar procedure (i.e. since the plate-boundary function is known, the normal to the boundary can be determined), but leads to

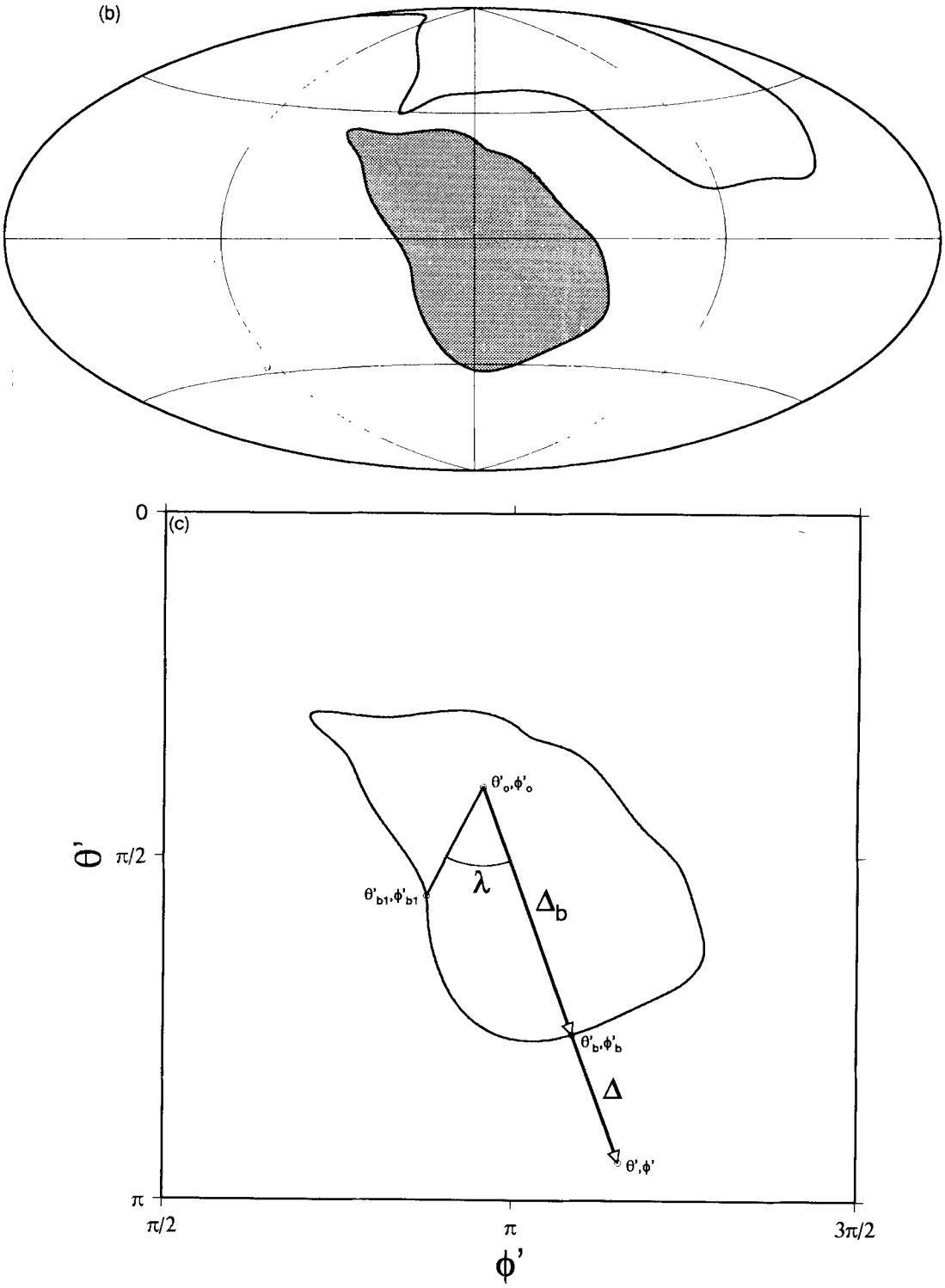

Figure 4. (*Continued.*)

considerably more complicated expressions. With the plate margin function δ^* determined, the plate-shape function (eq. 25) is complete.

In this model for the shape of a tectonic plate, the horizontal divergence D and radial vorticity ω_r of the plate's motion are analytically continuous. Since D and ω_r are scalars they are invariant to coordinate transformations. Thus D and ω_r at the transformed point (θ', ϕ') have the same values at the untransformed point (θ, ϕ) in the original (geographic) frame. (Naturally, the angular velocity vector $\boldsymbol{\Omega}$ must be rotated into the (θ', ϕ') frame for D and ω_r to be calculated.) D and ω_r for each plate depend on the derivatives of the shape function which are given in

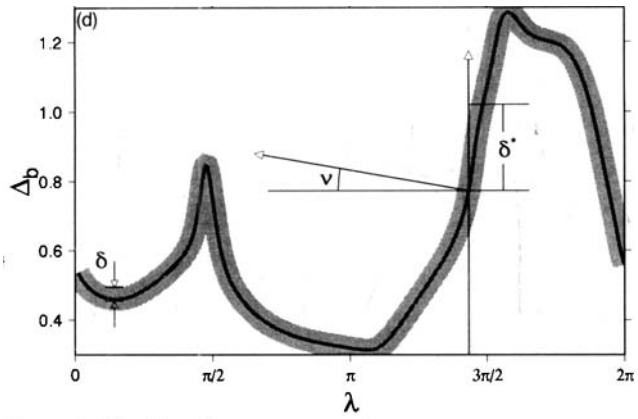

Figure 4. (*Continued.*)

abbreviated form as

$$\frac{\partial S}{\partial \chi^{\pm}} = \frac{1}{2\delta}\operatorname{sech}^2\left(\frac{\Delta_b - \Delta}{\delta\sqrt{1+(d\Delta_b/d\lambda)^2}}\right)\frac{1}{\sqrt{1+(d\Delta_b/d\lambda)^2}} \times\left[\frac{(\chi_0^{\pm}-\chi^{\pm})}{\Delta} \mp \frac{(\chi_0^{\mp}-\chi^{\mp})}{\Delta^2}\frac{d\Delta_b}{d\lambda} \times\left(1-\frac{[\Delta_b-\Delta]\,d^2\Delta_b/d\lambda^2}{1+(d\Delta_b/d\lambda)^2}\right)\right] \tag{28}$$

where $\chi^{+} = \theta'$, $\chi^{-} = \phi'$ and

$$\frac{d\Delta_b}{d\lambda} = \frac{1}{N}\sum_{n=-N/2}^{N/2} in\tilde{\Delta}_n e^{in\lambda} \tag{29}$$

$$\frac{d^2\Delta_b}{d\lambda^2} = -\frac{1}{N}\sum_{n=-N/2}^{N/2} n^2\tilde{\Delta}_n e^{in\lambda}. \tag{30}$$

Since the plate-boundary function $\Delta_b(\lambda)$ is approximated with a Fourier series, its derivatives are susceptible to Gibbs effects. These can be reduced with moderate Gaussian filtering; we empirically find that multiplying $\tilde{\Delta}_n$ by $e^{-n^2/N}$ in eqs (24), (29) and (30) yields satisfactory results. However, this *ad hoc* correction raises the question of why the convoluted method described so far is preferrable to spherical-harmonic analysis and appropriate spectral filtering (i.e. tapered truncation). First, filtering of spherical-harmonic series essentially imposes finite-width margins indirectly by an implied spatial convolution with some unknown plate shape (or plate-margin shape) model. In this paper, the plate margin structure and plate shape are specified directly in the physical domain; they are thus more physically grounded and are more capable of incorporating data on margin width and intraplate deformation. Second, in the method described here, enhancing resolution of the plate boundaries entails increasing the value of N for 12 linear Fourier series. To do the same with a spherical-harmonic expansion is more costly since resolution is essentially homogeneous (over the global surface) and must be increased everywhere when it is actually only the plate boundaries that need to be well resolved. Thus to increase the resolution by a factor M means increasing the size of the linear Fourier series in the method presented here by M, and by M^2 in the spherical-harmonic method.

The D and ω_r for all plates are added in the original geographic (θ, ϕ) reference frame, yielding the global divergence and vorticity fields, shown in Fig. 5 for $R\delta = 200$ km. As expected, the curvature of the boundaries is reduced. However, Gibbs effects (i.e. ringing) are eliminated. Several features hidden in the ringing of the spherical-harmonic representation of the discontinuous plate model (Fig. 3) appear clearly in the continuous model (Fig. 5). For example, the Phillipine plate is distinguishable in the vorticity field of the continuous plate model (compare to Fig. 3), and the divergent motion at its southern end (e.g. at the Ayu trough; see Weissel 1980), while invisible in the discontinuous plate model, is distinct in the continuous model.

The model described has certain advantages and disadvantages in comparison to the discontinuous plate-tectonic model. As discussed above, it is more mathematically well behaved for problems of plate-mantle coupling since it is essentially a continuum model of the plates. In addition to avoiding singularities (and associated numerical problems) the model crudely accounts for finite-margin width and (even more crudely) intraplate deformation. However, because the plate shapes must be manipulated and smoothed until they are analytically describable, the model loses information about small-scale tectonic features and causes gaps between the plates. The importance of these weaknesses can only be assessed *a posteriori* (and only incompletely) with comparison to the plate-tectonic model. Since all tectonic models are simplifications and approximate in nature, it is not a simple matter to determine which one is best as there is no absolute standard.

5.2 Results: energy partitioning and plate margin width

We use the model described above to examine the influence of plate margin width on the kinetic-energy partitioning for plates with (roughly) present-day motions and geometries. This exercise will indicate the dependence of partitioning on the plate-tectonic assumption (i.e. of rigid plates with discontinuous boundaries) and (crudely) the influence of intraplate deformation on partitioning.

Figure 6 shows the spherical-harmonic kinetic energy spectra for the discontinuous NUVEL-1 model to spherical-harmonic degree $\ell = 40$ (O'Connell, personal communication, 1992) along with the continuous model for plate margin width $R\delta$ between 40 km and 1000 km. With all of its simplifications, the continuous model preserves many of the primary features of the energy spectrum. Most notable is the local peak at spherical-harmonic degrees 4 and 5 and a smaller one at degree 8; these local maxima probably reflect basic plate geometries since they change little as plate-margin-width changes. The tracking of the poloidal energy spectrum by the toroidal one is also preserved in the continuous plate model. The low-order harmonics have essentially the same energies in both the discontinuous and continuous models (for all values of δ). The slope of the spectra at high wavenumbers, however, is affected by changes in δ. For the discontinuous model, kinetic energy falls off essentially as ℓ^2, which is expected for step functions (Hager & O'Connell 1978, 1979; O'Connell *et al.* 1991; Olson & Bercovici 1991) and implies that the spherical-harmonic representation of velocities is probably non-convergent (since the power spectra of the

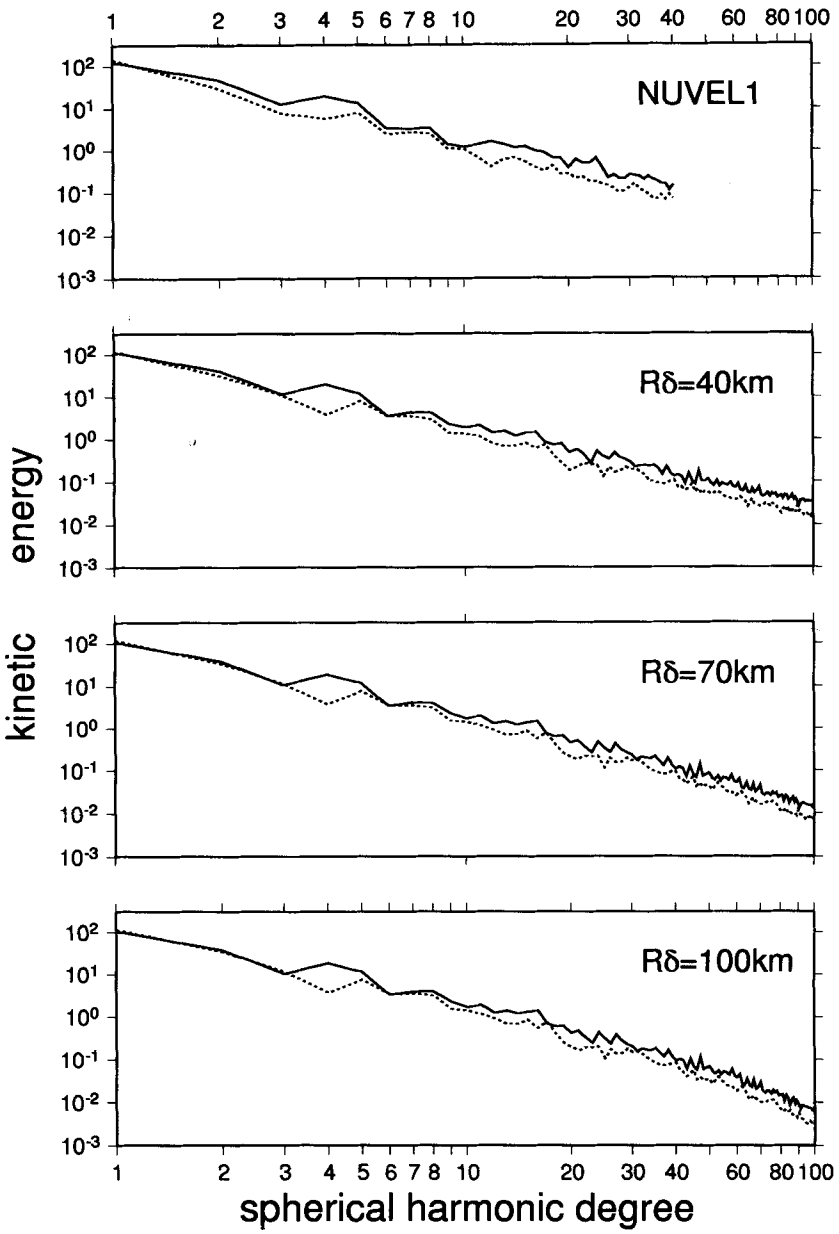

Figure 6. Spherical-harmonic kinetic-energy spectrum for the discontinuous plate-tectonic model (from analysis of the NUVEL-1 model to spherical-harmonic degree 40; O'Connell, personal communication, 1992) and the continuous plate model with plate margin half-width $R\delta$ ranging from 40 km to 1000 km. Solid lines indicate poloidal energy; dashed lines are toroidal energy. Units of energy are $(\text{rad/Gyr})^2$.

RMS velocities, or $\sqrt{KE_P + KE_T}$, fall off as $1/\ell$). For the continuous model, the energy spectrum falls off more rapidly with ℓ (but not as a power law) as the margin width increases to 400 km (Fig. 6). This trend is to be expected as the smoothing of the plate boundaries and use of continuous shape functions reduce high-wavenumber effects. Thus with the continuous model, velocities can be represented by convergent spherical-harmonic series, and hence ringing can be eliminated. However, as $R\delta$ increases past 400 km, the high-wavenumber tail of the spectrum begins to lift again. This reversal occurs because the increase in margin width eventually causes the plate interiors to become narrow features that induce high-wavenumber harmonics in the energy spectrum.

The total poloidal and toroidal kinetic energies and their ratio are shown as functions of margin width in Fig. 7; the energies from the NUVEL-1 discontinuous model are associated with $\delta = 0$. The kinetic energies decrease monotonically with increasing δ as expected, since an increase in margin width causes the amount of convergent–divergent and strike-slip motion to diminish. KE_T however, approaches an asymptote for large δ and eventually exceeds KE_P at $R\delta \approx 900$ km. Unlike KE_P, KE_T levels at large δ because of the contribution to spin: although an increase in margin width reduces the magnitude of convergence, divergence and strike-slip shear, it has relatively little effect on spin vorticity. KE_P thus approaches zero as δ increases, while KE_T does not. These relations obviously have significant effects on the energy partitioning in plate motion. The ratio KE_T/KE_P starts at less than unity for small δ and

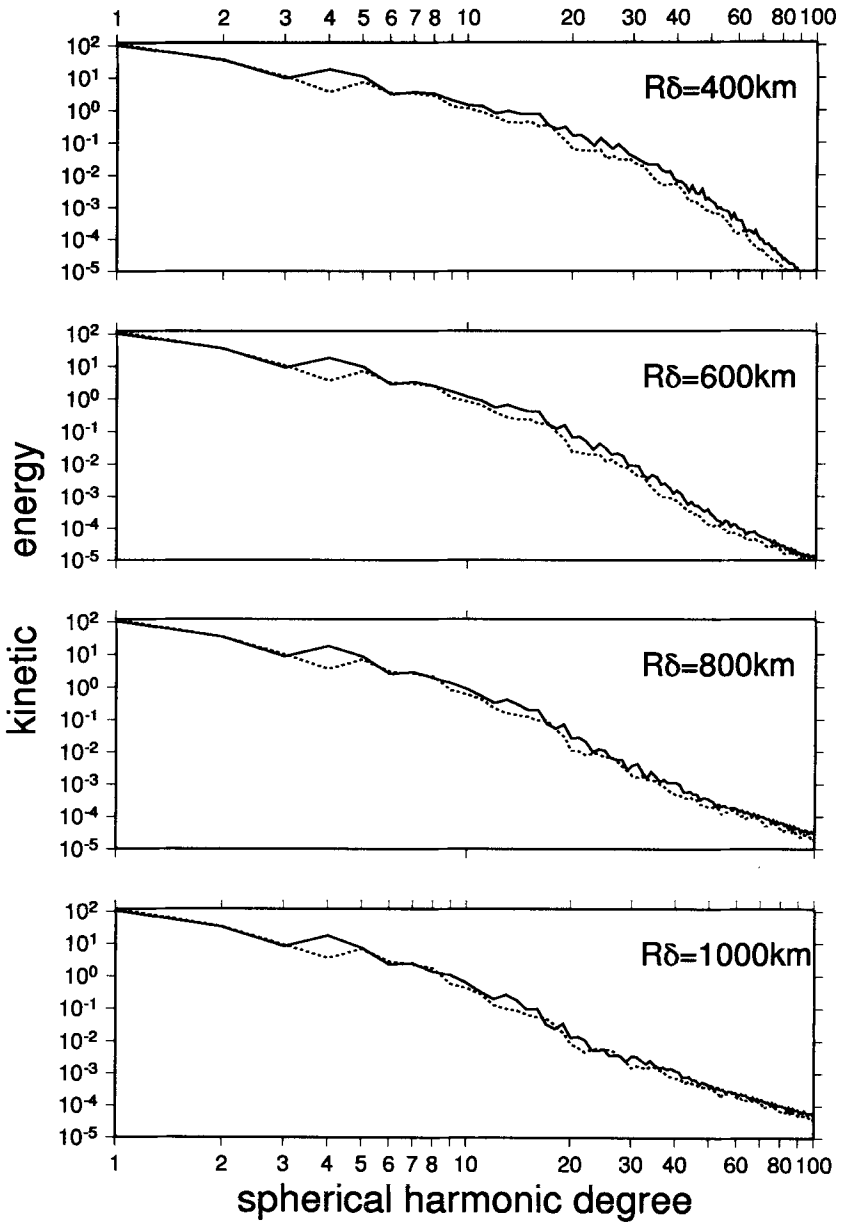

Figure 6. (*Continued.*)

increases with margin width, eventually exceeding unity (at $R\delta \approx 900$ km). (The small decrease in KE_T/KE_P from $R\delta = 0$ to $R\delta = 40$ km is likely due to underlying differences between the discontinuous and continuous models, e.g. exact plate geometries, choice of Pacific-hotspot pole, etc.) Accounting for finite plate margins (and thus intraplate deformation) may, therefore, change the relative proportions of toroidal and poloidal kinetic energies.

6 CONCLUSIONS

In this paper, we have proposed a simple kinematic theory of spatially continuous plate-tectonic motions. The proposed model essentially introduces finite margin width into the theory of plate tectonics by using analytically continuous shape functions to describe plate geometry. This model has advantages for the study of plate–mantle coupling as it allows the discontinuous theory of plate tectonics to be expressed in a continuum form that is more suited for the fluid-dynamic theory of mantle flow.

The plate model presented here was used to examine the influence of finite margin width on kinetic-energy partitioning. An examination of the relation between energy partitioning and plate geometry for idealized plates in a spherical geometry indicates that partitioning depends on plate size as well as aspect; in particular the larger a plate the more profound the contribution of spin vorticity to the toroidal energy. In the discontinuous plate-tectonic model, however, divergence and strike-slip shear are singularities, and hence tend to overwhelm the contribution from spin vorticity. When finite margin widths are allowed, the spin vorticity becomes significant (especially in the presence of large plates such as the Pacific) causing toroidal motion to assume a larger if not major portion of the kinetic energy.

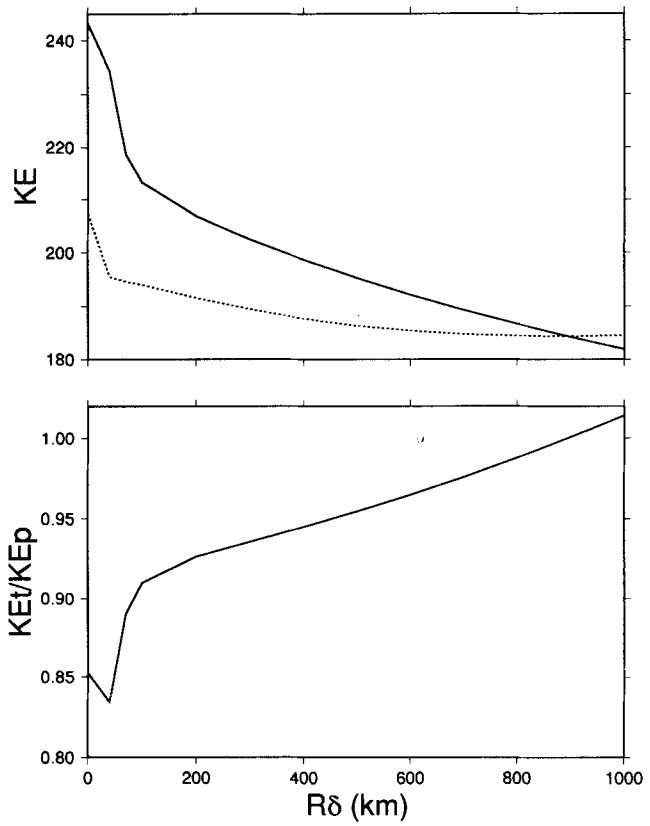

Figure 7. Total poloidal (solid curve) and toroidal (dashed curve) kinetic energies versus margin half-width $R\delta$ (top frame). The NUVEL-1 model analysis is used for the point corresponding to $R\delta = 0$. The energy ratio KE_T/KE_P is shown in the bottom frame.

The model calculations presented here, however, assume that all margins have essentially the same width. A rigorous estimate of the effect of finite margin width requires constraints from geodetic measurements of intraplate deformation. With the continuous plate model, the incorporation of data on plate margin widths and intraplate deformation is possible. One would essentially need to estimate the margin-width function $\delta^*(\lambda)$ for every plate from tectonic and geologic analyses. The actual structure of velocity profiles across the margins, however, could not be easily incorporated into the model, since it is not likely that simple analytic functions such as hyperbolic tangents would fit these profiles. More elaborate functions (e.g. splines) could be employed, at considerable expense and loss of simplicity.

It would also be desirable to model the plate shapes more realistically, i.e. use a smaller Gaussian-filter half-width for plate-boundary smoothing. The Indo–Australian plate boundary is the most difficult to represent by analytic single-valued functions and thus prescribes the minimum filter width. Recent work, however, has indicated a diffuse zone of deformation within this plate (Wiens *et al.* 1985; Gordon, DeMets & Argus 1990; DeMets *et al.* 1990). Resolution of this zone into a boundary separating the Indian and Australian plates would possibly facilitate more realistic plate shapes for all plates. Regardless of this potential improvement, the plate boundaries would still need to be smoothed to some degree, and thus small-scale information, e.g. the detailed structure of ridge offsets, would be lost. However, it should be emphasized that a continuous plate model is most useful in the study of large-scale global tectonics. In this context, therefore, a refinement of the model and incorporation of plate margin data would seem a worthy endeavour since the continued development of a continuous plate model is a necessary step toward making plate tectonics and mantle dynamics compatible.

ACKNOWLEDGMENTS

We are grateful to R. J. O'Connell for supplying his spherical-harmonic coefficients for the NUVEL-1 plate model, and to B. Taylor, R. N. Hey, and S. A. Weinstein for helpful advice. This work was supported by NASA through grant NAGW-3015 for DB and by NSF through grant OCE-92-2926 for PW. SOEST contribution number 3611.

REFERENCES

Bercovici, D., 1993. A simple model of plate generation from mantle flow, *Geophys. J. Int.*, **114,** 635–650.

Christensen, U. & Harder, H., 1991. Three-dimensional convection with variable viscosity, *Geophys. J. Int.*, **104,** 213–226.

DeMets, C., 1993. Earthquake slip vectors and estimates of present-day plate motions, *J. geophys. Res.*, **98,** 6703–6714.

DeMets, C., Gordon, R.G., Argus, D.F. & Stein, S., 1990. Current plate motions, *Geophys. J. Int.*, **101,** 425–478.

Forte, A.M. & Peltier, W.R., 1987. Plate tectonics and aspherical earth structure: the importance of poloidal–toroidal coupling, *J. geophys. Res.*, **92,** 3546–3680.

Gable, C.W., O'Connell, R.J. & Travis, B.J., 1991. Convection in three dimensions with surface plates: generation of toroidal flow, *J. geophys. Res.*, **96,** 8391–8405.

Gordon, R.G., DeMets, C. & Argus, D.F., 1990. Kinematic constraints on distributed lithospheric deformation in the equatorial Indian ocean from present motion between the Australian and Indian plates, *Tectonics*, **9,** 409–422.

Hager, B.H. & O'Connell, R.J., 1978. Subduction zone dip angles and flow driven by plate motion, *Tectonophysics*, **50,** 111–133.

Hager, B.H. & O'Connell, R.J., 1979. Kinematic models of large-scale flow in the Earth's mantle, *J. geophys. Res.*, **84,** 1031–1048.

Hager, B.H. & O'Connell, R.J., 1981. A simple global model of plate dynamics and mantle convection, *J. geophys. Res.*, **86,** 4843–4867.

Kaula, W.M., 1980. Material properties for mantle convection consistent with observed surface fields, *J. geophys. Res.*, **85,** 7031–7044.

Kaula, W.M. & Williams, D.R., 1983. Transformations of velocity fields on a spherical surface, in *Geodesy in Transition*, pp. 177–183, eds Schwarz, K.P. & Lachapelle, G., University of Calgary, Alta.

King, S.D., Gable, C.W. & Weinstein, S.A., 1992. Models of convection-driven plates: a comparison of methods and results, *Geophys. J. Int.*, **109,** 481–487.

Lithgow-Bertelloni, Richards, M.A., Ricard, Y., O'Connell, R.J. & Engebretson, D.C., 1993. Toroidal–poloidal partitioning of plate motions since 120Ma, *Geophys. Res. Lett.*, **20,** 375–378.

Minster, J.B. & Jordan, T.H., 1978. Present-day plate motions, *J. geophys. Res.*, **83,** 5331–5354.

Minster, J.B., Jordan, T.H., Molnar, P. & Haines, E., 1974.

Numerical modelling of instantaneous plate tectonics, *Geophys. J. R. astr. Soc.*, **36,** 541–576.

Morgan, W.J., 1968. Rises, trenches, great faults, and crustal blocks, *J. geophys. Res.*, **73,** 1959–1982.

O'Connell, R.J., Gable, C.W. & Hager, B.H., 1991. Toroidal–poloidal partitioning of lithospheric plate motion, in *Glacial Isotasy, Sea Level and Mantle Rheology*, pp. 535–551, eds Sabadini, R. *et al.*, Kluwer Academic Publishers, Dordrecht.

Olson, P. & Bercovici, D., 1991. On the equipartitioning of kinetic energy in plate tectonics, *Geophys. Res. Lett.*, **18,** 1751–1754.

Olson, P. & Corcos, G.M., 1980. A boundary layer model for mantle convection with surface plates, *Geophys. J. R. astr. Soc.*, **62,** 195–219.

Pollitz, F.F., 1988. Episodic North American and Pacific plate motions, *Tectonics*, **7,** 711–726.

Ribe, N.M., 1992. The dynamics of thin shells with variable viscosity and the origin of toroidal flow in the mantle, *Geophys. J. Int.*, **110,** 537–552.

Ricard, Y. & Vigny, C., 1989. Mantle dynamics with induced plate tectonics, *J. geophys. Res.*, **94,** 17 543–17 559.

Ricard, Y., Froidevaux, C. & Fleitout, L., 1988. Global plate motion and the geoid: a physical model, *Geophys. J.*, **93,** 477–484.

Weinstein, S. & Olson, P., 1992. Thermal convection with non-Newtonian plates, *Geophys. J. Int.*, **111,** 515–530.

Weissel, J.K., 1980. Evidence for Eocene oceanic crust in the Celebes Basin, in *The Tectonic and Geologic Evolution of Southeast Asian Seas and Islands*, pp. 37–47, ed. Hayes, D.E., Geophys. Monogr. 23, Am. geophys. Un., Washington, DC.

Wiens, D.A., DeMets, C., Gordon, R.G., Stein, S., Argus, D., Engeln, J.F., Lundgren, P., Quible, D., Stein, C., Weinstein, S. & Woods, D.F., 1985. A diffuse plate boundary model for Indian Ocean tectonics, *Geophys. Res. Lett.*, **12,** 429–432.